Belt Conveyor Idler Fault Detection System Based on an uwDAS Cable-Fiber Optic Microphone Combination

TANG Xu1#; ZHANG Mengmeng1#

1. College of Mathematics and Physics, Hubei Engineering Research Center of Weak Magnetic-Field Detection, China Three Gorges University, Yichang 443002, China

Abstract: To address the demand for belt conveyor idler fault detection under strong interference and long-distance operating conditions, this paper proposes an ultra-weak fiber Bragg grating distributed acoustic sensing (uwDAS) detection system that combines point-type fiber optic microphones with distributed optical cable. Fiber optic microphones are deployed in strong-vibration areas such as motors and hoppers, while sensing cable is laid at close range along the outside of the conveyor belt. The system acquires idler signals along the entire conveyor without blind zones. Variational mode decomposition (VMD) denoising and time-frequency analysis are used to verify the feasibility of idler fault detection. Experiments show that in the 100-2000 Hz range, the designed fiber optic microphone improves average sound-pressure sensitivity by 21 dB re 1 rad/μPa compared with a bare fiber coil. In idler fault tests, both the fiber optic microphone and cable detect fault signals; the microphone achieves an SNR of 0.71 dB, higher than the 0.01 dB of the cable. The method combines the long-distance coverage of sensing cable with the high sensitivity of fiber optic microphones, improving fault detection at key locations while maintaining flexible deployment. It provides a reliable technical approach for belt conveyor fault detection.

Keywords: ultra-weak FBG distributed acoustic sensing; fiber optic microphone; sound pressure sensitivity; fault detection; variational mode decomposition

Figure and Table Captions

1. Introduction

A belt conveyor is a friction-driven mechanical system consisting of a drive device, conveyor belt, tensioning device and idlers. It is widely used for material transport in coal mines, gravel, fertilizer and other scenarios. Idlers support the belt and are the core components that enable material transport. They are also the most numerous components in the system and account for about one-third of the total machine weight.

Idlers operate for long periods under high load and dusty conditions and are prone to faults such as jamming and damage. Such faults may lead to belt deviation, wear and even tearing, causing unplanned shutdowns and safety risks. Because idlers are numerous and densely distributed, fault detection is challenging. The timing and severity of idler failures are random, and the probability of failure increases with service time. Efficient, real-time and reliable idler detection is therefore important for personnel safety and stable industrial operation.

Conventional idler condition detection mainly relies on manual walking inspection, which is inefficient, time-consuming and labor-intensive, and carries risks of injury and hearing damage. Robot inspection depends on environmental modeling for localization and path planning, increasing system complexity and deployment cost. Fiber-optic sensing is passive, supports long-distance transmission, is immune to electromagnetic interference and can be distributed along the monitored structure. Distributed acoustic sensing has shown value in rail transit, oil and gas pipelines and power facilities.

Traditional interferometric DAS systems often have low SNR, limited spatial resolution and high cost. Ultra-weak FBG-based distributed acoustic sensing (uwDAS) provides clear advantages. Because UW-FBGs have extremely low

reflectivity, they reduce spectral shadowing and greatly improve sensing-network multiplexing, allowing multiple gratings to be connected on a single fiber and expanding the application range of fiber sensing.

Previous studies have used DAS and distributed fiber-optic sensing to monitor belt conveyor idlers and related industrial equipment. However, DAS signal quality depends heavily on fiber installation, and vibrations from adjacent idlers can cause crosstalk. This paper proposes an uwDAS cable-fiber optic microphone system for idler fault detection. In regions near the discharge port where materials scatter and accumulate and cable installation is difficult, point-type fiber optic microphones are installed to reduce the risk of cable damage. In areas with less material scattering, uwDAS cable is laid to realize long-distance, continuous monitoring of conveyor idler conditions.

2. Principle

2.1 uwDAS Cable-Fiber Optic Microphone Sensing System

The hybrid sensing system consists of optical cable, fiber optic microphones, a demodulation module and a computer. The cable serves as the backbone for signal transmission and distributed baseline sensing. Fiber optic microphones are fusion-spliced in series with the cable at key regions as local sensitivity-enhanced units. The demodulation module recovers disturbance information by demodulating the phase of Fizeau interference between reflected lights from adjacent gratings.

When sound waves act on the fiber, they cause tiny strain and change the optical phase. The uwDAS system demodulates this phase change to reconstruct key parameters such as sound amplitude and frequency. The computer collects grating phase data through host software at a sampling rate of 10 kHz. When sound or vibration acts on the cable, microstrain is induced in the cable, modulating the optical pulse phase and enabling detection of acoustic or vibration events. Coiling the cable during installation increases the effective sensing length affected by sound or vibration and enhances the response to weak signals.

The secondary sensitivity-enhanced fiber optic microphone consists of a shell, mandrel and base. A foam sensitivity-enhancing material with Young's modulus of about 16.5 MPa and Poisson's ratio of about 0.35 is attached to the mandrel surface, and bend-insensitive fiber is wound on the foam with prestrain to form the sensing core. The mandrel is fixed on the base, and the base is embedded into the shell to form the microphone.

The mandrel-shell design realizes secondary sensitivity enhancement. First, sound enters through the acoustic holes and acts on the mandrel, which deforms slightly and strains the wound fiber. Second, the shell reflects part of the sound wave back to the mandrel. Early reflections act again on the mandrel and increase deformation amplitude, improving weak-signal response. The rigid mandrel provides structural stability and raises resonance frequency, while the low-modulus foam generates larger deformation under sound pressure and significantly increases sensitivity.

By combining fiber optic microphones with distributed cable, the system retains long-distance continuous sensing and adds high-sensitivity detection at key local regions.

2.2 Variational Mode Decomposition

Variational mode decomposition (VMD) is a fully non-recursive and adaptive signal-processing method. It constructs and solves a variational problem to obtain the optimal center frequency and finite bandwidth of each mode component, enabling effective signal decomposition. Each mode is assumed to have finite bandwidth around a center frequency, and the goal is to minimize the sum of estimated bandwidths under the constraint that all modes sum to the original signal.

The Hilbert transform is applied to each mode to obtain analytic signals, and each mode spectrum is shifted to baseband. The squared gradient norm is calculated to estimate bandwidth. By introducing a Lagrange multiplier and quadratic penalty term, the constrained variational problem is converted to an unconstrained one. The alternating direction method of multipliers (ADMM) is then used to iteratively update the mode functions, center frequencies and Lagrange multiplier until convergence.

Selecting the optimal intrinsic mode function (IMF) is key for reconstruction and denoising. For fiber optic microphone signals, a composite index combining envelope entropy and envelope spectrum kurtosis is introduced. Envelope entropy reflects signal sparsity; if an IMF contains more noise and less feature information, its entropy is larger. Envelope spectrum kurtosis characterizes the prominence of fault-characteristic peaks and is sensitive to impulsive components. A larger composite index indicates richer fault information and lower noise interference.

For cable signals, kurtosis is used as the primary selection criterion because it is sensitive to transient impact components and can identify impulsive features from background noise. Since the cable is fixed on the idler frame and is easily affected by low-frequency vibration, kurtosis helps select the IMF containing impact components and avoids low-frequency noise interference.

3. Experiments and Results

3.1 Fiber Optic Microphone Performance Test

The microphone performance test system included an uwDAS demodulator, computer, audio signal generator, sound-level meter, bare fiber coil, fiber optic microphone, vibration-isolation sponge and sound-absorbing box. The bare fiber coil served as the control group, and the coil and microphone were different grating points on the same fiber. Both were placed on a flat sponge and inside the sound-absorbing box to reduce external vibration and echo.

The audio generator produced sine signals from 100 Hz to 2000 Hz in 50 Hz steps. For each frequency, the phase information demodulated by uwDAS and the sound pressure recorded by the meter were captured. The ratio of phase to sound pressure was the sound-pressure sensitivity. In the 100-2000 Hz range, the average sound-pressure sensitivities of the fiber optic microphone and bare fiber coil were -117.6 dB re 1 rad/μPa and -138.6 dB re 1 rad/μPa, respectively. The microphone improved average sensitivity by 21 dB re 1 rad/μPa.

3.2 Belt Conveyor Fault Detection System

The field experiment was conducted in the industrial park of Yichang Aneng Biomass Thermal Power Co., Ltd., on the No. 1 and No. 2 material conveyor belts with a total length of 100 m. Fiber optic microphones were installed near the discharge port where material scattering was severe, and cables were laid in other regions. Both were arranged longitudinally along the conveyor and fixed to idler brackets with cable ties to form a complete distributed detection system.

The discharge-port region showed severe material scattering and accumulation. Installing fiber optic microphones there replaces cable laying and prevents cable damage, while cable is installed in regions less affected by materials. Faulty idlers usually produce knocking or impact sounds clearly different from normal operation. To obtain fault signals, a steel pipe was used to lightly jam a normally operating idler and generate abnormal sound, simulating an idler fault condition.

3.3 Idler Fault Signal Processing

Idler fault signals are nonstationary and nonlinear. Short-time Fourier transform depends on a fixed window and wavelet transform depends on a basis function, both of which limit time-frequency resolution. Empirical mode decomposition is adaptive but can suffer mode mixing and end effects. VMD is introduced because it adaptively determines the center frequency and finite bandwidth of each intrinsic mode by solving a variational problem, enabling robust decomposition of nonstationary and nonlinear signals.

3.3.1 Selection of VMD Mode Number k

The center frequency of each mode is the key to distinguishing modes, so k can be selected by comparing modal center frequencies. Ideally, the center frequencies should be well separated. If two modes have close center frequencies, decomposition is poor or over-decomposition has occurred. Stable-operation signals were analyzed after excluding conveyor startup and shutdown. For microphone signals, k = 4 was selected based on center-frequency separation, Pearson correlation coefficients and the index of orthogonality. For cable signals, the same selection method indicated k = 5.

3.3.2 Time-Frequency Analysis

Time-domain waveforms of fiber optic microphone and cable signals under normal and faulty idler conditions were analyzed using stable-operation data from 4 s to 24 s. After normalization, it was difficult to distinguish normal and faulty conditions in the time domain, so frequency-domain analysis was required.

Fast Fourier transform showed that the cable had larger low-frequency amplitude, while the fiber optic microphone had lower low-frequency response. This is because the cable is fixed to the idler bracket and is directly affected by low-frequency bracket vibration. The microphone senses acoustic signals and is less sensitive to bracket vibration due to its stable mandrel structure and prestrained sensing fiber.

In the frequency spectrum, the cable fault signal showed peaks near 880 Hz and 1100 Hz, while the microphone fault band was near 1000-1200 Hz. Because the cable and microphone measured different idlers, their fault bands differed. Since fault signals were mixed with environmental noise, VMD denoising was used. For microphone signals, the IMF with the largest composite index was selected; for cable signals, the IMF with the largest kurtosis was selected.

After denoising, the fiber optic microphone signal showed more obvious amplitude fluctuation than the cable signal. The calculated SNR was 0.71 dB for the microphone and 0.01 dB for the cable, indicating that microphone signals after denoising have a significantly better signal-to-noise ratio and stronger fault detection capability.

Short-time Fourier transform was used for further analysis because FFT lacks time resolution. The low-frequency energy difference between normal and fault conditions was not obvious, while high-frequency energy differed significantly. The microphone showed much lower low-frequency energy than the cable, indicating less interference from low-frequency vibration. After VMD denoising, noise energy in the fault signal was suppressed and the fault frequency

band was retained. The idler fault center frequency was around 1000 Hz. The analysis confirms that the proposed uwDAS cable-fiber optic microphone system can detect idler faults effectively while combining the distributed advantage of cable and the local sensitivity enhancement of microphones.

4. Conclusion

This paper proposes an idler fault detection system based on an uwDAS cable-fiber optic microphone combination. Fiber optic microphones are deployed at critical local nodes, while cable is laid in other regions to realize long-distance continuous coverage.

First, the microphone structure significantly improves local sound-pressure sensitivity. Laboratory tests show that in the 100-2000 Hz range, the average sensitivities of the microphone and bare fiber coil are -117.6 dB re 1 rad/μPa and -138.6 dB re 1 rad/μPa, respectively. The sensitivity enhancement improves the ability to capture weak fault signals and provides a sensing basis for early fault identification at critical regions.

Second, field tests verify that both uwDAS cable and fiber optic microphones can detect idler fault signals. Analysis of data from a belt conveyor field site shows that after VMD denoising, both the microphone and cable detect fault signals effectively, demonstrating system validity and engineering applicability under practical conditions.

Third, the system can flexibly allocate the ratio and position of cable and fiber optic microphones according to different test scenarios, and has good universality and scalability. The validated field conditions and fault types are still limited, and fault-feature extraction and recognition methods require further optimization.

Translated Tables

Table 1. Center frequencies for different k values

k	Mode 1	Mode 2	Mode 3	Mode 4	Mode 5	Mode 6
2	50.8	682.2				
3	69.7	565.6	694.3			
4	69.5	565.5	694.3	3440.1		
5	63.9	553.2	683.2	1005.9	3453.4	
6	63.8	553.2	683.2	1005.8	3447.1	4267.5

Table 2. Correlation coefficients between each mode and the original signal

k	IMF1	IMF2	IMF3	IMF4	IMF5	IMF6
2	0.653	0.806				
3	0.439	0.664	0.729			
4	0.438	0.664	0.729	0.060		
5	0.430	0.630	0.773	0.0140	0.0003	
6	0.430	0.630	0.773	0.2940	0.0510	0.0002

Table 3. Index of orthogonality values under different k values

k	2	3	4	5	6
IO	0.1020	0.0888	0.0877	0.0994	0.1030

References

Reference entries are retained in the original citation form to avoid altering source bibliographic data.

当声波或振动作用于光缆时，会使光缆产生微小应变，从而调制光脉冲的相位，实现对声波振动事件的感知。而在实际铺设中对光缆进行打圈处理，能增加该处声波或振动作用于光缆的有效传感长度，累积更多相位变化，增强光缆对微弱信号的响应能力。

二次增敏机理的光纤麦克风，其结构由外壳、芯轴和底座三部分组成。支撑芯轴表面贴合杨氏模量约为 16.5 MPa 和泊松比约为 0.35 的泡沫增敏材料，抗弯光纤以一定的预应力缠绕在泡沫增敏材料上构成光纤麦克风芯轴，光纤麦克风芯轴固定在光纤麦克风底座上，光纤麦克风底座严密内嵌于光纤麦克风外壳，构成光纤麦克风。光纤麦克风采用芯轴-外壳设计实现二次增敏。首先，声波经过外壳上的拾音孔直接作用于芯轴，芯轴发生微小形变并带动缠绕在芯轴上的光纤产生应变，实现一次增敏；其次，光纤麦克风外壳能够有效反射声波，部分经过光纤麦克风外壳反射的声波再次作用于芯轴[18]。根据光纤麦克风尺寸与声速粗略估计当反射时间小于 50 ms 时属于早期反射[19]。早期反射再次作用于芯轴，有效增强芯轴的形变幅度，实现二次增敏，进一步提高对弱信号的响应能力。较硬的支撑芯轴为光纤麦克风

提供较好的稳定性能，能够有效防止结构在长期振动下的变形，同时提升系统的整体谐振频率，拓宽其频率响应的带宽；而泡沫增敏材料具有较低的杨氏模量和泊松比，在声压作用下可以产生较大的形变量，从而显著提高了灵敏度。

该系统在光缆长距离、连续性的感知基础上，通过光纤麦克风与光缆的组合，实现长距离覆盖检测与关键区域高灵敏度检测的兼顾。

图 1 uwDAS 的光缆–光纤麦克组合检测系统结构示意图 (1)外壳；(2)芯轴；(3)底座

Fig. 1 System schematic of an uwDAS-based hybrid detection system integrating optical cables and FOMs.(1) shell; (2) Mandrel; (3) Base.

2.2 变分模态分解

变分模态分解[20]是一种完全非递归、自适应的信号处理方法，该方法通过构造、求解变分问题的最优解，获取每个模态分量的最佳中心频率和有限带宽，实现对信号的有效分解。变分问题的构造如下：

（1）假设每个模态都是具有中心频率的有限带宽，问题可描述为寻找()个模态函数，使得每个模态的估计带宽之和最小，其约束条件为各个模态之和等于原信号。

（2）对每个模态函数进行希尔伯特变换，得到解析信号。

其中为单位脉冲函数。然后将各模态信号与相乘，将模态频谱调制到相应基频带，即：

其中为中心频率在复平面上的相量描述，为第个本征模态函数的中心频率。

（3）计算以上信号梯度的平方范数，算出各模态的信号带宽之和，最终得到受到约束的变分问题表示如下：

式中为需要分解的模态个数，表示分解生成的个 IMF 分量，表示每个 IMF 分量的中心频率，并且所有分量总和满足；为卷积运算符；为求偏导；表示为所有模态数的总和。

求解变分问题时，引入 Lagrange 乘法算子和二次惩罚项，将约束变分问题转化为非约束变分问题，得到的增广 Lagrange 表达式为

利用交替方向乘子(alternate direction method of multipliers,ADMM)进一步解决变分问题，通过迭代更新、和，寻找增广拉格朗日表达的“鞍点”，获得约束变分模型的最优解，和表示迭代次数。在迭代过程中，为方便计算，将、转到频域，可得到二次型问题的解为：

从式(5)中可以看出，从频谱开始确定 VMD 的分解模态数，本征模态函数从频谱上可以看作围绕迭代优化得到的波峰。此外，可看作为的剩余信号的维纳滤波。

利用相同原理解决的最小值问题，将此问题转到频域求解，固定与，中心频率更新为模态功率谱的重心，获得中心频率；通过对偶上升强化重构约束，获得拉格朗日算子：

其中、和分别为、和的傅里叶变换；为保真系数。从原信号中分离 IMF 中，每个 IMF 分量的频率中心和带宽不断更新，直至满足迭代停止条件，如式(8)所示

其中为收敛精度。最后对求解出的模态求逆傅里叶变换就得到了经过 VMD 分解后得到的各个模态的时域形式。

如何从 VMD 分解出的模态分量中选取最优 IMF 是重构降噪的关键一步。光纤麦克风信号 VMD 分解中 IMF 分量的选取规则，引入贺[21]等人提取的包络熵和包络谱峭度相结合的复合指标，计算公式为

包络熵代表原始信号的稀疏特性，当 IMF 中噪声较多，特征信息较少时，则包络熵值较大，反之，则包络熵值较小[22]。为表征解调后包络谱中故障特征峰的突出程度，弥补包络熵在表征冲击信号熵的不足，引入包络谱峭度指标。已有研究[23]将谱峭度引入包络谱分析框架中，利用其对冲击性成分的敏感性增强故障特征的可检测性。当 IMF 包含的故障信号和冲击信号越多，峭度值就越大，反之则越小。光纤麦克风主要采集声音信号，使用复合指标能够筛选出最优的 IMF。复合指标越大，表明该 IMF 分量所包含的故障信息越丰富，同时受噪声干扰越小。

对于光缆信号 VMD 分解中 IMF 分量的选取规则，采用峭度指标作为核心判断依据。这是因为峭度[24]对信号中的瞬态冲击成分十分敏感，能够有效从含背景噪声的信号中识别出瞬态冲击特征及其在频带中的分布。光缆固定在托辊保持架上，易受低频振动干扰，峭度能直接筛选出含冲击成分的 IMF，避免被低频噪声干扰。计算公式如下：

式中：为输入的信号；为的均值；为采样信号的长度；是的标准差。

3. 实验与结果

3.1 光纤麦克风性能测试

光纤麦克风性能测试系统如图 2(a)所示，包括 uwDAS 解调设备、电脑、音频信号发生器、声压计、裸纤环、光纤麦克风、减震海绵和吸音箱。其中，裸纤环为光纤麦克风的对照组，二者为一根光纤上的不同栅点。在测试时，将裸纤环和光纤麦克风放在平坦的减震海绵上，一起放入吸音箱中，以减小外界振动和回音的干扰。将传感光纤与 uwDAS 解调设备连接，uwDAS 解调设备连接电脑实时显示测试信号。电脑驱动音频信号发生器，产生所需的声波信号，并使声波沿光纤麦克风径向入射，声压计放置在与光纤麦克风同等声压的地方，用于记录声压。音频信号发生器生成 100~2000 Hz 频率范围内的正弦信号，以 50 Hz 为步长，分别记录每个频率下 uwDAS 解调出的相位信息以及对应声压计的数值，相位与声压的比值即为该频率下的声压灵敏度。裸纤环和光纤麦克风的声压灵敏度随频率的变化曲线，如图 2(b)所示。在 100~2000 Hz 频率范围内光纤麦克风和裸纤环的平均声压灵敏度分别为-117.6 dB re 1 rad/uPa 和-138.6 dB re 1 rad/uPa，光纤麦克风相较于裸纤环，平均声压灵敏度提高了 21 dB re 1 rad/uPa。

图 2 光纤麦克风性能测试 (a)光纤麦克风频率响应测试装置结构示意图；(b)光纤麦克风和裸纤环的频率响应曲线图

Fig. 2 FOMs performance testing. (a) Schematic diagram of the frequency response test device structure for the FOMs; (b) Frequency response curves of the FOMs and the bare fiber coil

3.2 皮带机故障检测系统

本实验在宜昌安能生物质热电有限公司的工业园内，总长为 100 m 的 1 号与 2 号运料皮带机上进行。在物料散落严重的下料口区域布设光纤麦克风，其余区域铺设光缆。二者均沿皮带机纵向排布，并使用扎带固定在托辊保持架上，构成完整的分布式检测系统。皮带机现场、光纤麦克风布设和光缆铺设如图 3 所示。由图 3 可知，皮带机下料口区域存在严重的物料散落与堆积现象，这是该区域的固有特点，将光纤麦克风布设于此，可替代该区域的光缆铺设，从而避免光缆铺设在该区域受损，其余受到物料影响较小的区域则铺设光缆。托辊出现故障时，通常会发出敲击声或撞击声，与正常托辊的运行声音存在明显区别。若托辊发生故障不及时更换，会导致皮带撕裂甚至出现发热起火的危险情况。为研究故障声音特征以实现托辊故障检测，需要获取托辊故障信号。为此，本研究采用人工模拟方法制造对比样本：使用钢管轻微卡住正常运行中的托辊，使其产生区别于正常状态的异响，从而模拟托辊故障工况。

图 3 皮带机现场及光纤麦克风、光纤布设图 (a)uwDAS 系统电脑；(b) 1、2 号运料皮带机；(c) 铺设的光缆；(d) 布设的光纤麦克风

Fig. 3 The layout of the belt conveyor site and the arrangement of FOMs and optical cables (a) Host computer of the uwDAS system; (b) No. 1 and No. 2 material-conveying belt conveyors; (c) Installed optical cables ; (d) Deployed FOMs

3.3 托辊故障信号处理

托辊发生故障时，其产生的信号呈现出非平稳、非线性的特征。对于非平稳、非线性信号的分析，传统短时傅里叶变换依赖固定窗函数，小波变换依赖基函数，二者存在时频分辨率受限的问题。经验模态分解(empirical mode decomposition,EMD)虽具自适应性，但容易出现模态混叠、端点效应等问题。为了解决上述方法存在的问题，引入变分模态分解。它是一种完全非递归、自适应的信号处理方法，其核心在于通过构造并求解变分问题，自适应地确定每个本征模态的最佳中心频率与有限带宽，从而实现对非平稳、非线性信号的精准、稳健分解。

3.3.1 变分模态数 k 值选取

模态中心频率的大小是区分每个模态的关键，因此可以通过观察对比每个模态的中心频率的方法确定值的选取[25]。理想状态下各模态分量的中心频率应相互分离，若出现中心频率较为相近的模态分量，则说明分解效果不佳。排除皮带机启动和停止的影响，选取稳定运行阶段的信号进行分析，确定信号全局的值。光纤麦克风信号选取不同值进行 VMD 分解，惩罚因子为默认值 2000，保真系数为 0.2，对应的中心频率如表 1 所示。从表 1 中可以看出，=5 时，有两个变分模态分量的中心频率为 683.2 Hz 和 1005.9 Hz，相距较近；在=6 时，这两个模态分量的中心频率变化不大，相距较近，可认为已出现过分解。而=4 时，这两个模态分量的中心频率为 694.3 Hz 和 3440.1 Hz，相距较远，因此模态数选 4 较为合适。

表 1 不同值各模态的中心频率

Tab.1 Center frequencies corresponding to different k values

不同值下，VMD 分解后的各模态与原信号的皮尔逊相关系数(pearson correlation coefficient,P)，如表 2 所示。当=4 时，相关系数为 0.060，=5 时，相关系数为 0.0003、=6 时，相关系数为 0.0002。这说明当大于 4 时，模态 5、6 的相关系数将变得很小，可判断出该模态为虚假模态，因此模态数选取 4，可在充分提取有效故障特征的同时，避免由过分解产生的虚假模态。

表 2 不同值下各模态与原信号间的相关系数

Tab.2 Correlation coefficients between each mode and the original signal under different k values

同时，EMD 分解中，利用正交性性能指标(index of orthogonality,IO)定量分析原信号的分解精度问题。值可用于衡量所有不同 IMF 之间相互干扰与能量耦合程度，其值越小，表明分解出的各模态分量越独立，正交性越好，分解效果就越好。正交性性能指标定义如下：

式中，和为不同阶次的模态分量，表示信号长度。

表 3 为不同值下，光纤麦克风信号 VMD 分解的值。可以看到当=4 的时候值最小，当>4 或者<4，值都会增大。表 1 中，当=3 时，565.6Hz 和 694.3Hz 这两个模态分量距离更近，但模态间能量耦合程度较大，对应表 3 中值(0.0888)大于=4 时的值(0.0877)，说明分解效果不佳。因此，综合上述三个选取原则，可以判断出选取 4 时较为合适。

表 3 不同值各模态的值

Tab.3 values under different k values

对光缆信号的 VMD 模态数的确定，采用同样的选取方式，选取 5 较为合适。

3.3.2 时频域分析

托辊正常与托辊故障状态下，光纤麦克风和光缆采集的信号时域图如图 4 所示。选择稳定运行阶段 4-24 s 期间的数据进行分析，并进行归一化消除幅值的影响。光纤麦克风和光缆信号在时域里面很难区分托辊正常与托辊故障，需要进一步在频域分析。

图 4 光纤麦克风和光缆信号时域图 (a)光纤麦克风-托辊正常；(b)光纤麦克风-托辊故障；(c) 光缆-托辊正常；(d)光缆-托辊故障

Fig. 4 Time domain waveforms of the FOMs and optical cables signals (a) FOMs-idler under normal condition; (b) FOMs-idler fault; (c) optical cables-idler under normal condition; (d) optical cables-idler fault.

对上述托辊正常与故障的光纤麦克风和光缆信号进行傅里叶变换(fast fourier transform,FFT)，得到的频谱如图 5 所示。可以发现，光缆在低频附近幅值较大，而光纤麦克风较小。这是因为光缆通过轧带固定在托辊保持架上，皮带机运行期间产生的振动传递到托辊保持架，直接作用于光缆，受到低频振动分量影响，低频幅值增加。而光纤麦克风内部传感光纤以一定预应力紧密缠绕在光纤麦克风芯轴，光纤麦克风芯轴固定于芯轴固定底座上，这使得光纤麦克风内的传感光纤有更强的结构稳定性，并且光纤麦克风采集的是声音信号，对保持架低频振动不够敏感，其低频幅值较小。对比托辊正常与托辊故障，光缆采集的托辊故障信号频段在 880Hz 和 1100Hz 附近有两个尖峰，而光纤麦克风采集的托辊信号故障频段在 1000-1200Hz 附近。由于光缆与光纤麦克风的信号采集对象为不同托辊，因此其 FFT 故障频段有差异，并且故障信号往往与环境噪声混杂，需要使用 VMD 降噪处理，再结合两类信号的筛选 IMF 原则，选出最优的 IMF，实现故障信号的重构降噪。

图 5 光缆与光纤麦克风托辊信号频谱图 (a)托辊正常；(b)托辊故障

Fig. 5 Fourier Transform Spectra of Sensing Cable and FOM Signals for Idlers: (a) Normal; (b) Faulty.

为了更直观地比较光纤麦克风和光缆对托辊故障的响应差异，对上述故障信号进行 VMD 分解，在分解得到的 IMF 中，光纤麦克风信号依据复合指标最大原则(式 9)选取 IMF 分量，而光缆信号则依据峭度(式 10)最大原则选取 IMF 分量，以实现对不同信号下故障特征的针对性提取与对比分析。降噪结果如图 6 所示。

图 6 托辊故障信号 VMD 降噪前后对比：(a)光纤麦克风；(b)光缆

Fig. 6 Comparison of idler fault signals before and after VMD denoising: (a) FOMs; (b) Optical cables

观察图 6 可以看到，故障信号降噪后，光纤麦克风相较于原信号幅值波动更明显而光缆较为平缓。计算其信噪比(signal-to-noise ratio,SNR)，SNR 的计算公式为：

式中，为原始信号；为 VMD 降噪后的信号；为数据长度。光纤麦克风 SNR 为 0.71 dB，而光缆 SNR 为 0.01 dB。这表明，在托辊故障检测中，光纤麦克风采集的信号经过降噪后，其信噪比显著优于光缆信号，具备更优的故障检测能力。

传统傅里叶变换因缺乏时间分辨率，无法定位敏感频率成分的出现时刻；而短时傅里叶变换(Short-time fourier transform,STFT)可在时频域上同时表征信号的频率分布与时间。因此利用短时傅里叶变换进一步分析。光纤麦克风、光缆短时傅里叶变换图如图 7 所示，光纤麦克风和光缆采集到托辊信号，其低频能量在正常和故障差异不明显，而高频能量差异显著。光纤麦克风低频能量明显低于光缆低频能量，说明其受到低频振动信号干扰更少。

图 7 光纤麦克风、光缆短时傅里叶图 (a) 光纤麦克风-托辊正常；(b) 光纤麦克风-托辊故障(c)光纤麦克风-托辊故障信号 VMD 降噪后；(d) 光缆-托辊正常；(e)光缆-托辊故障正常；(f)光缆-托辊故障信号 VMD 降噪后

Fig. 7 Short-time Fourier transform spectrograms of the FOMs and the optical cables. (a) idler under normal condition measured by the FOMs; (b) idler fault measured by the FOMs; (c) FOMs fault signal after VMD based denoising; (d) idler under normal condition measured by the optical cables; (e) idler fault measured by the optical cables; (f) optical cables fault signal after VMD based denoising.

另一组光纤麦克风、光缆信号的短时傅里叶图如图 8 所示。

图 8 另一组光纤麦克风、光缆短时傅里叶图 (a)光纤麦克-托辊正常；(b)光纤麦克风-托辊故障；(c)光纤麦克风-托辊故障 VMD 降噪后；(d)光缆-托辊正常；(e)光缆-托辊故障；(f)光缆-托辊故障 VMD 降噪后

Fig. 8 another Short-time Fourier transform spectrograms of the FOMs and the optical cables. (a) idler under normal condition measured by the FOMs; (b) idler fault measured by the FOMs; (c) FOMs fault signal after VMD based denoising; (d) idler under normal condition measured by the optical cables; (e) idler fault measured by the optical cables; (f) optical cables fault signal after VMD based denoising.

观察发现低频成分在托辊正常和故障差异不明显，而高频成分差异显著。当出现故障时，虚线框内能量相较于正常状况显著增加，VMD 降噪后故障信号中噪声能量被有效抑制，仅仅保留故障频段。结合图七可知托辊故障信号中心频率在 1000 Hz 附近。由于不是同一个托辊故障信号，因此两组光纤麦克风与光缆信号的 VMD 降噪后重构的故障信号中心频率有轻微区别。图 5 的 FFT 图像大致确定光纤麦克风与光缆采集到托辊故障频段的所在，但受到环境噪声影响无法判断具体位置，同时 FFT 仅反映频域的整体能量分布，无法捕捉时频域的动态细节。图 7、8 中(a)(b)(d)(e)不仅直观展示托辊正常与故障的频率段差异，(c)(e)还能直观看到 VMD 降噪后故障特征频段的具体分布，弥补了 FFT 在时频分析上的不足。

综合上述分析，所提出 uwDAS 光缆-光纤麦克风的托辊故障检测系统，不仅能够实现托辊故障的有效检测，还兼顾光缆的分布式优势与光纤麦克风的局部增敏性，实现皮带机全链路的长距离检测。同时光纤麦克风采集声学信号，在皮带机强振动环境下对振动不敏感，对托辊故障声音信号灵敏，有利于提高诊断结果的稳定性和可靠性。

4. 结 论

本文提出了一种基于 uwDAS 光缆-光纤麦克风的托辊故障检测系统。在局部关键节点布设光纤麦克风，其他部位铺设光缆从而实现长距离、连续覆盖式检测，具体结论如下：

(1)光纤麦克风结构显著提升了局部声压灵敏度。实验室测试结果表明，在 100–2000 Hz 频率范围内，光纤麦克风与裸纤环的平均声压灵敏度分别为−117.6 dB re 1 rad/μPa 和 −138.6 dB re 1 rad/μPa，光纤麦克风结构相较于裸纤环实现了明显的灵敏度提升，有效增强了系统对微弱故障信号的捕捉能力，为关键区域早期故障识别提供了传感基础。需要指出的是，本研究现场验证的工况与故障类型相对有限，且故障特征提取与识别方法仍有进一步优化空间。

(2)现场试验验证了 uwDAS 光缆与光纤麦克风对托辊故障的检测能力。基于宜昌安能生物质热电有限公司工业园的皮带机现场采集数据分析表明，经 VMD 降噪处理后，光纤麦克风与光缆均能有效地检测到托辊故障信号，验证了系统在实际工况下的有效性与工程适用性。

(3)此系统可根据不同测试场景，合理分配光缆与光纤麦克风的布设比例与位置，具备良好的通用性、可扩展性。

参考文献:

[1] Alharbi, Fahad,Luo, Suhuai,Zhang, Hongyu , et al.A Brief Review of Acoustic and Vibration Signal-Based Fault Detection for Belt Conveyor Idlers Using Machine Learning Models[J].Sensors,2023,23,(4):1902..

[2] Shiri, Hamid,Wodecki, Jacek,Zietek, Bartlomiej , et al.Inspection Robotic UGV Platform and the Procedure for an Acoustic Signal-Based Fault Detection in Belt Conveyor Idler[J].Energies,2021,14,(22):7646.

[3] Du, Yuxin,Zhang, He,Liang, Liang , et al.Applications of Machine Vision in Coal Mine Fully Mechanized Tunneling Faces: A Review[J].IEEE Access,2023,11,102871-102898

[4] Piotr Bortnowski,Witold Kawalec,Robert Król , et al.Types and causes of damage to the conveyor belt – Review, classification and mutual relations[J].Engineering Failure Analysis,2022,140.

[5] Szrek, Jaroslaw,Jakubiak, Janusz,Zimroz, Radoslaw.A Mobile Robot-Based System for Automatic Inspection of Belt Conveyors in Mining Industry[J].Energies,2022,15(1):327.

[6] David Milne,Ali Masoudi,Edgar Ferro , et al.An analysis of railway track behaviour based on distributed optical fibre acoustic sensing[J].Mechanical Systems and Signal Processing,2020,142,

[7] Jinpeng Jiang,Fang Liu,Honghai Wang , et al.Lateral positioning of vibration source for underground pipeline monitoring based on ultra-weak fiber Bragg grating sensing array[J].Measurement,2021,172.

[8] Chai, Quan,Luo, Yang,Ren, Jing , et al.Review on fiber-optic sensing in health monitoring of power grids[J].Optical Engineering,2019,58,(7).

[9] Wenjing GAO,Jianxia LIU,Huiyong GUO , et al.Multi-Wavelength Ultra-Weak Fiber Bragg Grating Arrays for Long-Distance Quasi-Distributed Sensing[J].Photonic Sensors,2022,12,(2):185-195.

[10] Liang Kun, Wang Chi. Roller fault monitoring of belt conveyor using distributed fiber-optic acoustic sensor [J]. Laser & Optoelectronics Progress, 2023, 60(9): 266-74.

[11] Xie, Miao,Li, Bo,Ma, Suning , et al.Research on roller monitoring technology based on distributed fiber optic sensing system[J].Scientific Reports,2024,14,(1):1-17.

[12] Wijaya H, Rajeev P, Gad E, Vivekanamtham R. Distributed optical fibre sensor for condition monitoring of mining conveyor using wavelet transform and artificial neural network [J]. Structural Control and Health Monitoring, 2021, 28(11): e2827.

[13] Hua Zheng,Huan Wu,Hao Yin , et al.Novel mining conveyor monitoring system based on quasi-distributed optical fiber accelerometer array and self-supervised learning[J].Mechanical Systems and Signal Processing,2024,221.

[14] Bai, Yu,Xie, Peng,Liu, Chong , et al.Experimental Study on Spontaneous Combustion Monitoring in Coal Mine Airspace Based on Distributed Fiber Optic Temperature Measurement[J].Combustion Science and Technology,2025,197,(17):4477-4497.

[15] Hua Li,Xing Wu,Tao Liu , et al.Composite fault diagnosis for rolling bearing based on parameter-optimized VMD[J].Measurement,2022,201, 111637.

[16] Ho, Hsiang-Wei,Liao, Wei-Hsiang,Chang, Ching-Yuan , et al.Structural health monitoring of a linear robot by fiber Bragg grating sensors and cyber-physical system[J].The International Journal of Advanced Manufacturing Technology,2022,122,(9-10):3983-3995.

[17] LUO Z, YANG Z, LU B, et al. Modular DAS demodulation system based on ultra-weak fiber Bragg grating[J]. Journal of Instrumentation, 2022, 17(10): P10037.

[18] Ran, Changyan,Zhang, Mengmeng,Luo, Zhihui , et al.A Secondary Sensitivity-Enhanced Fiber-Optic Microphone Based on Ultra-Weak Fiber Bragg Grating[J].IEEE Transactions on Instrumentation and Measurement,2025,74.

[19] Kowalczyk, Konrad.Raking early reflection signals for late reverberation and noise reduction[J].The Journal of the Acoustical Society of America,2019,145,(3):EL257-EL263.

[20] K. Dragomiretskiy, D. Zosso, Variational Mode Decomposition[J], IEEE Trans. Signal Process. 62 (3) (2014) 531–544.

[21] HE Z J, LI J X, LIU S W , et al. Roller bearing fault diagnosis combined CEEMD-VMD and parameter optimization SVM [J]. Mechanical Science and Technology for Aerospace Engineering, 2024, 43(3): 402-8.

[22] TANG G J, WANG X L. Parameter optimized variational mode decomposition method with application to incipient fault diagnosis of rolling bearing [J]. Journal of Xi'an Jiaotong University, 2015, 49(5): 73-81.

[23] Ahmed Intekhab Rohan,Tasfia Akter Ridita,Hasanur Zaman Anonto , et al.Intelligent fault diagnosis in rolling element bearings: Combining envelope spectrum and spectral kurtosis for enhanced detection[J].Results in Engineering,2025,27,1-14.

[24] XUE Y, CHEN Z G, WANG Y.X, et al. Fault feature extraction of rolling bearing based on VMD optimized by composite spectral kurtosis [J]. Electronic Measurement Technology, 2024, 47(9): 1-7.

[25] QIAO M Y, LIU Y X, LAN J Y. Fault diagnosis method of rolling bearings based on VMD and mahalanobis distance SVM [J]. Acta scientiarum naturalium universitatis sunyatseni, 2019, 58(5): 8-16.

作者简介：(通信作者，要求应为指导教师)

姓名（出生年—），性，，，明（士/博士生导师），主要从事.....方面的研究。

Retained Figures and Visual Materials

The original figures, screenshots, diagrams and experimental plots from the source manuscript are retained below in their original order for layout continuity. Captions in the translated body follow the source numbering where available.

Original visual material 1

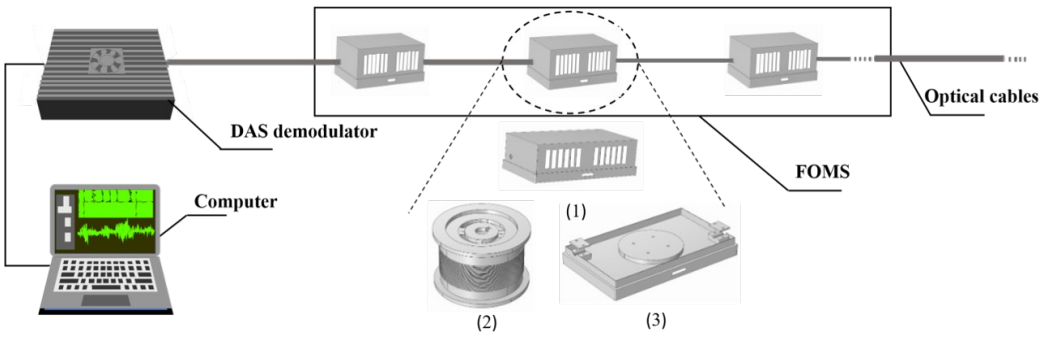

Original visual material 2

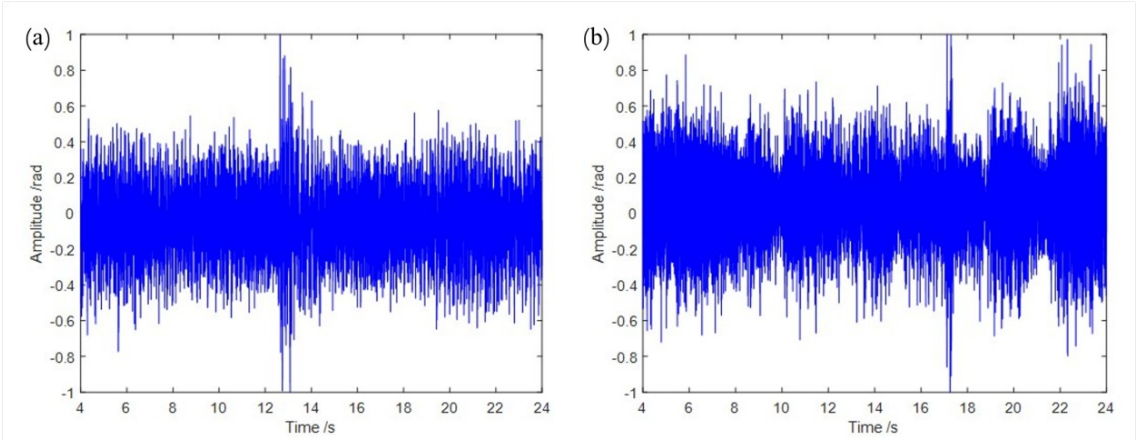

Original visual material 3

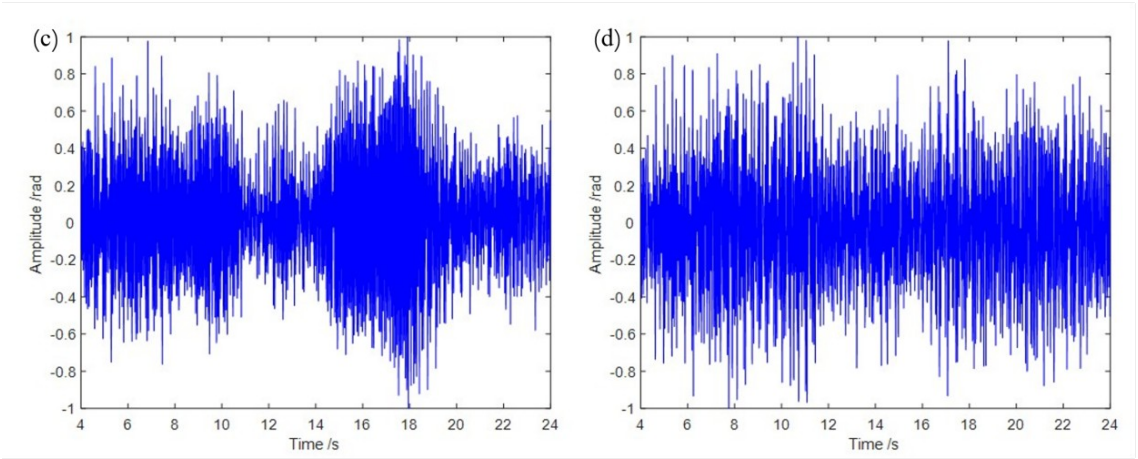

Original visual material 4

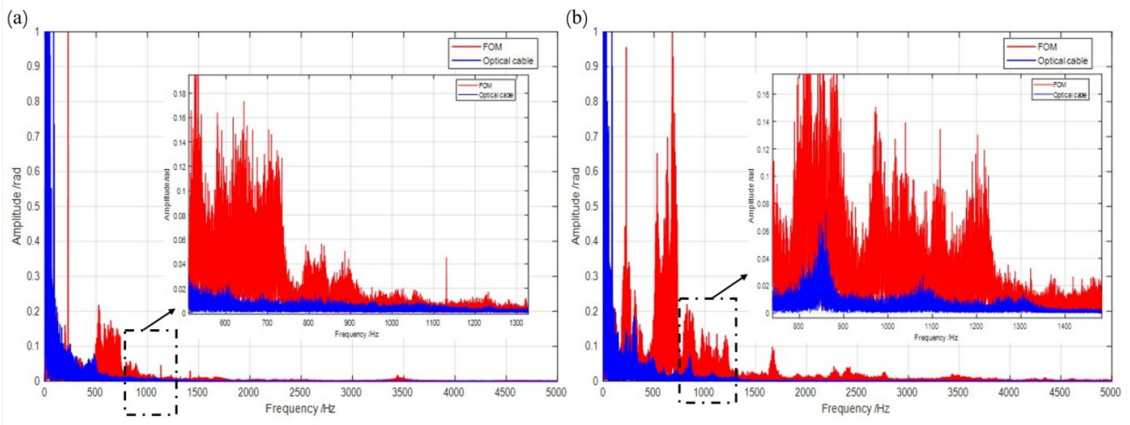

Original visual material 5

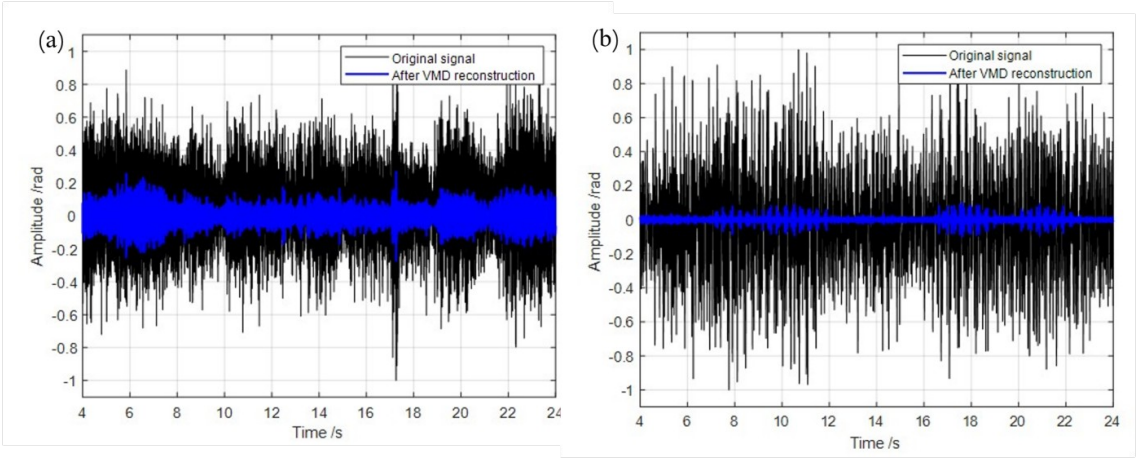

Original visual material 6

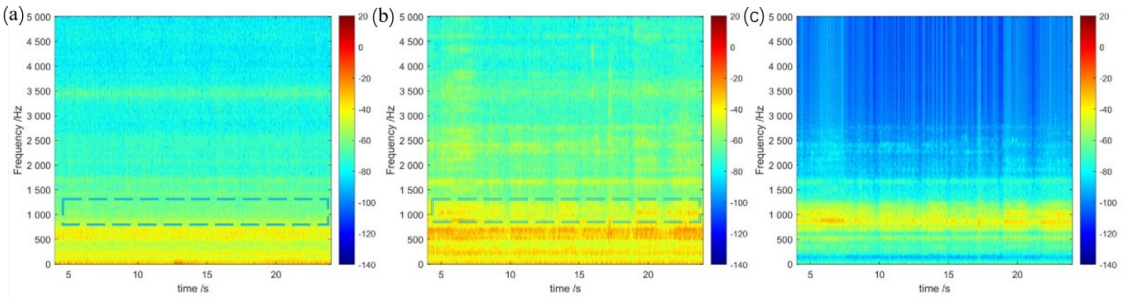

Original visual material 7

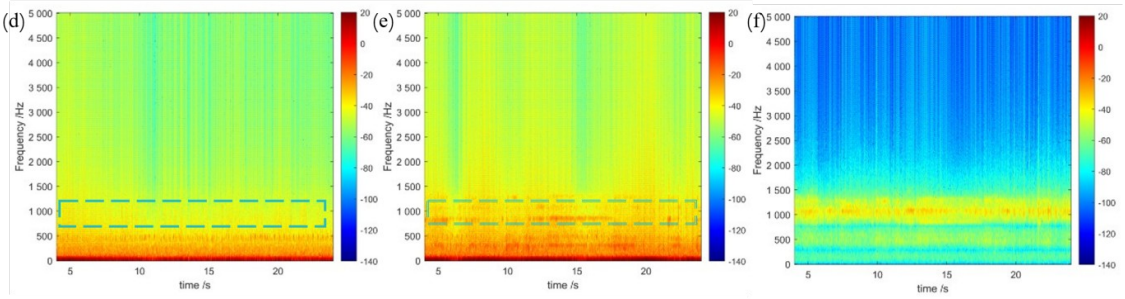

Original visual material 8

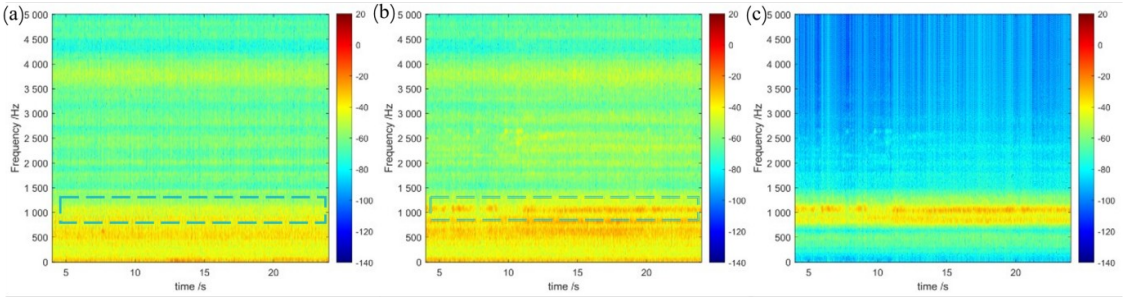

Original visual material 9

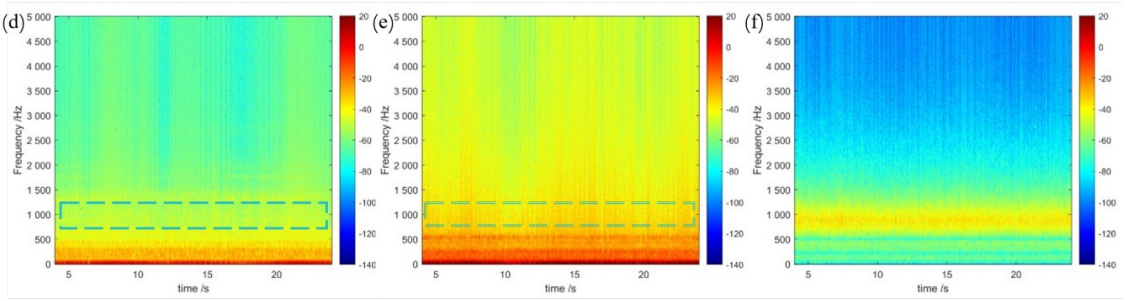

Original visual material 10

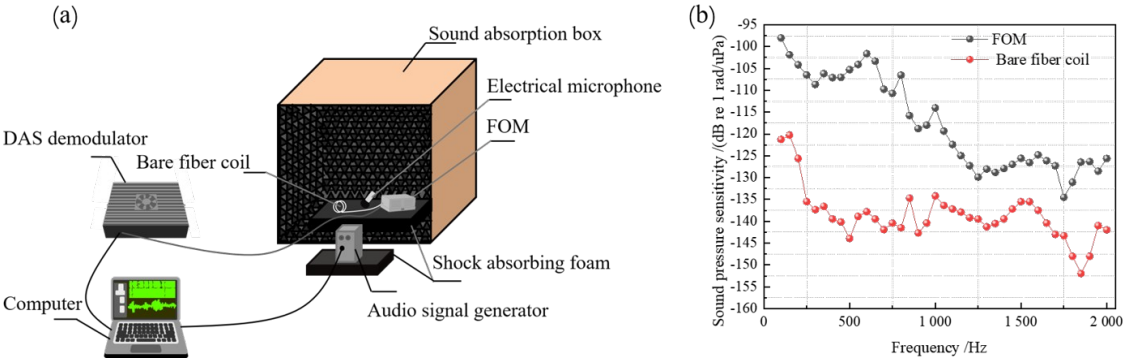

Original visual material 11